Solid Freeform Fabrication 2021: Proceedings of the 32nd Annual International Solid Freeform Fabrication Symposium – An Additive Manufacturing Conference
Reviewed Paper

Residual Stress Measurements via X-ray Diffraction Cos α Method on Various Heat-Treated Inconel 625 Specimens Fabricated via Laser-Powder Bed Fusion

Mohanish Andurkar[1], Toshikazu Suzuki[2], Masanao Omori[2], Bart Prorok[3], John Gahl[4], Scott Thompson[1, *]

[1]Alan Levin Department of Mechanical and Nuclear Engineering, Kansas State University, Manhattan, Kansas, USA, 66506

[2]Pulstec Industrial Co., Ltd., Hamamatsu, Shizuoka, Japan

[3]Department of Materials Engineering, Auburn University, Auburn, Alabama, USA, 36849

[4]University of Missouri Research Reactor (MURR), University of Missouri, Columbia, Missouri, USA, 65211

*Corresponding author: smthompson@ksu.edu

Abstract

The residual stress and hardness of Inconel 625 fabricated using Laser Powder Bed Fusion (L-PBF) were experimentally investigated. As-built Inconel 625 samples were subjected to three different heat-treatment temperatures of 700 ºC, 900 ºC, 1050 ºC for one hour. Effects of these three-stress relieving heat treatment temperatures on the nature and value of residual stress were studied. Residual stress measurements were recorded using a portable X-ray system. The system calculated residual stress using the cos α method. The Full Width Half Maximum (FWHM) of diffraction peaks in all samples were measured. The results indicate that tensile residual stress was present on the surface of as-built L-PBF sample and compressive residual stress on the surface of heat-treated samples due to stress relief. Debye-Scherrer (D-S) ring positions were measured using the cos α method and compared with a reference wrought Inconel 625 ring position. Vickers microhardness and residual stress were found to be positively correlated.

KEYWORDS: FWHM, Selective laser melting, Microhardness, Nickel superalloy, Additive manufacturing

Introduction

Metal additive manufacturing (AM) has been flourishing over the past few decades as it provides a means to build parts with complex geometry, reduced mass, and unique microstructural and mechanical properties. Laser Powder Bed Fusion (L-PBF), a metals AM technique, uses a high energy laser to melt a thin layer of powder, track by track, atop a build plate (and subsequently additional powder layers and solidified metal). Following a CAD design and pre-AM slicing software instructions, the laser selectively melts the thin powder layer causing powder particles to fuse with previously solidified layers of the part. Subsequent melting and solidifying of all thin layers ultimately build the desired 3-D geometry. Despite all

opportunities offered by AM, metal parts fabricated via AM can possess defects arising from high thermal gradients, temperatures, and cooling rates. Defects include lack of fusion, porosity, and inclusions. The steep thermal gradients often result in the formation of significant residual stress fields which can lead to warping, cracking, and distortion. Hence, the formation of residual stress presents a major challenge of adopting AM metals in fields like aerospace and nuclear industry where high dimensional accuracy and mechanical performance is expected.

Inconel 625 is a nickel-based superalloy that is notoriously hard to process via conventional methods due to its extreme hardness resulting from γ" and δ precipitation at high temperatures, low thermal conductivity, low elastic modulus, and abrasive chips. In addition, formation of secondary phases in nickel-based superalloys make it tougher resulting in tool wear during machining [1], [2]. For these reasons, many industries/users are looking at AM for processing nickel-based superalloys. Inconel 625 is used to build critical parts in harsh environments like aerospace, nuclear reactors, where a high level of mechanical strength is expected within cryogenic to very high temperatures. Previous studies have been conducted to estimate the magnitude of residual stress in Inconel-series materials built in different orientations via AM. Wang and Chou investigated residual stresses formed in Inconel 718 produced via Electron Beam Additive Manufacturing (EBAM) and Selective Laser Melting (SLM) using the mechanical instrumented indentation technique [3]. They found tensile and compressive residual stresses in the plane parallel and the plane normal to build direction, respectively, within the SLM-built Inconel 718. Liu et al. studied the residual stress formation in Inconel 718 fabricated by L-PBF employing the Vicker micro-indentation method. They observed a positive correlation between tensile residual stress and microhardness [4]. In addition, Barros et al. analyzed residual stress in L-PBF-built Inconel 718 before and after heat treatment using a hole-drilling strain-gage method. They observed the presence of tensile residual stress on the top surface of as-built specimens while compressive residual stress existed on the top surface of solution annealed heat-treated specimens [5]. Liu et al. measured residual stress in L-PBF parts made from gas atomized 316L stainless steel powder and demonstrated that the residual stress in the build direction is higher than that in the perpendicular direction within the material [6]. Smaller scan vector lengths used during L-PBF generally result in reduction of temperature gradients and residual stress [7]. In addition to mentioned techniques to reduce residual stress, preheating the build platform and heat treatment of as-built samples are also feasible solutions [8][9][5].

In general, measurements of residual stress can be performed via various methods and devices. Two major types of methods are destructive and non-destructive. Destructive methods involve removal of a small portion of the part to understand the relaxation of residual stress. Some examples of destructive methods are hole drilling, core drilling, stripping, and the contour method. Destructive testing methods are comparatively easy to execute and provide accurate results, but surface destruction can be unacceptable when assessing critical components. To prevent such surface damage, non-destructive methods have been introduced and developed. Non-destructive methods can involve X-ray, neutrons, synchrotron radiation, and magnetic strain [10]. X-ray diffraction (XRD) is widely preferred to measure residual stress along or near a surface due to its low penetration depth. Neutron diffraction methods provide volumetric stress fields because of its high penetration depth. Masoomi et al. used neutron diffraction to measure the residual stress distribution in L-PBF stainless steel 17-4 PH. The study required several hours of neutron exposure at specific regions along the samples. It was found that heat treating vertically-built cylinders reduces compressive axial stress in the core region [11].

XRD typically relies on using the $\sin^2\Psi$ method for calculating stresses. The XRD-$\sin^2\Psi$ stress method begins with XRD scans along series of defined incident angles (Ψ) over a pre-determined diffraction angle. From the scans performed at each incident angle, the selected diffraction peak position must be accurately verified, i.e., the 2θ value must be measured from a very wide-ranging and sometimes unevenly shaped peak. The obtained 2θ values are then used to execute the linear regression to obtain the slope and intercept values to be used for the stress calculation. Line detectors are usually used in the $\sin^2\Psi$ method which captures a small part of the Debye-Scherrer (D-S) ring at every incident angle (Ψ). The D-S ring is created by a diffraction pattern occurring due to Braggs law when X-rays are incident on a polycrystalline material. Recently, the cos α method, where α represents the azimuthal angle, has gained attention as a new method to measure residual stress. The cos α method employs the entire D-S ring produced from single exposure of X-rays at a single incident X-ray beam angle captured by a 2-D detector. The cos α method has several advantages over the traditional $\sin^2\Psi$ method such as simple optical setup and faster in-plane normal and shear stress calculations [12]. Past studies have proven the reliability of the cos α method by comparing measured residual stress values with those obtained via the traditional $\sin^2\Psi$ method [12][13][14]. Another important parameter obtained from the cos α method is the Full Width at Half-Maximum (FWHM) of the X-ray diffraction (XRD) peak under consideration. This FWHM parameter can be used to understand the state of a material surface's micro strain, grain morphology, and dislocation density.

The aim of this paper is to measure the surface residual stresses of as-built and heat-treated Inconel 625 samples fabricated using L-PBF. The cos α method is used to determine residual stress by capturing the D-S ring from a single exposure to X-rays. Residual stress is calculated by using the D-S ring distortion from standard Inconel 625 and comparing it with the radius of the D-S ring of the as-built and heat-treated Inconel 625 samples. Heat treatment was carried out on the as-built Inconel 625 samples using three different temperatures for one hour each. The in-plane residual stress, shear stress, and FWHM for all samples was calculated using cos α method and the results are presented. The Vickers microhardness of all samples and its relationship with residual stress is also investigated. The effects of heat-treatment temperatures on the value and nature of surface residual stress are provided, as well.

Methods

Gas atomized Inconel 625 powder with a mean particle diameter of 31.3 µm for L-PBF was sourced from Carpenter Technologies. Inconel 625 samples were built using a Concept Laser Mlab 100R commercial L-PBF system. This L-PBF system had a 100 W fiber laser at a wavelength of 70 nm. Fabrication was carried out in an enclosed high-purity argon atmosphere to avoid any oxidation while also providing a uniform supply of powder. The elemental composition (in % wt) of the employed, virgin Inconel 625 powder is as follows: Ni-Bal, Cr-21, Mo-9, Fe<5, Nb+Ta-3.5, Co<1.0, Al<0.4, Ti<0.4, Mn<0.5, and C<0.1. The elemental composition complies with the ASTM Standard for Additively Manufacturing Nickel Alloy UNS N06625. Inconel 625 samples were additively manufactured using process parameters as follows: power = 90 W, scan speed = 800 mm/s, laser diameter = 80 µm, layer thickness = 25 µm, and hatch spacing = 80 µm. These parameters were found to produce samples with 99.8% density. Cube Inconel 625 samples of size 10 mm^3 were built using the above-mentioned L-PBF process parameters. All samples were built in the vertical direction and an island scanning strategy was used with a checkerboard pattern consisting of 5 × 5 mm squares. Each island consisted of scan tracks that alternated in opposite directions. The as-built Inconel 625 samples were heat treated at three different temperatures of 700 ºC, 900 ºC, and 1050 ºC for 1 hour

each. The rationale for using these temperatures was to study how residual stress varies with the precipitation of the $\gamma''$and δ phases, as well as with recrystallization of grains in the additively manufactured Inconel 625 [15]. The heating rate used during heat treatment was ~5 ºC/min. All three heat-treated samples were exposed to air cooling to bring their temperatures to ambient temperature while remaining in the furnace. Uncertainty in heat treatment temperatures is ± 5 ºC. For experimental control and baselining, wrought Inconel 625 plate (152.4 x 152.4 x 4.76 mm^3) was acquired from Metalmen, NY, USA. The plate was produced per AMS5599. Small 1 x 1 x 0.5 mm samples were sectioned from the plate using wire electrical discharge machining (EDM).

The XRD technique is most common technique to measure near surface residual stress as the penetration depth of X-ray is low – on-the-order of 10 µm. In this study, residual stress measurements were carried out using a portable Pulstec µ-X360 X-ray system. The samples were irradiated using a beam current of 0.66 mA and voltage of 30 kV. The X-ray beam was directed to be incident on each sample at an angle of 28.8 degrees. The distance from the specimen and detector to capture the D-S ring image was set to D = 50 mm. The X-ray Manganese (Mn) *K*-alpha wavelength (λ) used for X-ray diffraction was 2.10 Å. The diffraction angle (2θ) was calculated using Bragg's law, i.e.:

$$n\lambda = 2d\sin\theta \tag{1}$$

where *n* is an integer and *d* is the d-spacing or interplanar spacing equal to 1.077 Å in this case. Using the above values, the diffraction angle was calculated as 155.03 degrees.

The µ-X360 X-ray Pulstec system utilizes a cos α technique to calculate in-plane residual stress (σ_x) and shear residual stress (τ_{xy}) as presented in Fig 1(a). Keeping the angle of incident X-rays constant, the relative position of the D-S ring for the L-PBF parts (red ring) from that of the wrought part distortion D-S ring (black ring) was used to calculate strain as presented in Fig 1(b). The equations used to calculate the in-plane stress and shear stress from strains are presented in Eqs. (2)-(5). The fundamental equations used to find the D-S ring radius and residual stress for this method are explained in detail in Refs. [12][16]. The (311) family of crystallographic planes were used to create the D-S rings and for verifying the residual stress in as-built and heat-treated samples, as the (311) planes represent bulk macro stresses and are less sensitive to intergranular strain compared to other planes. In addition, the sensitivity of peak broadening under the influence of external stress becomes higher with higher 2θ angles, thus, the use of diffraction peaks at higher 2θ angles provides a better option for conducting FWHM analysis [17]. Since a high level of tensile residual stress is generated at the top surface of the L-PBF samples due to the layer-wise AM process, the top oriented surface of each sample (surface facing upward during printing) was inspected to study the effects of heat-treatment temperature on residual stress and FWHM.

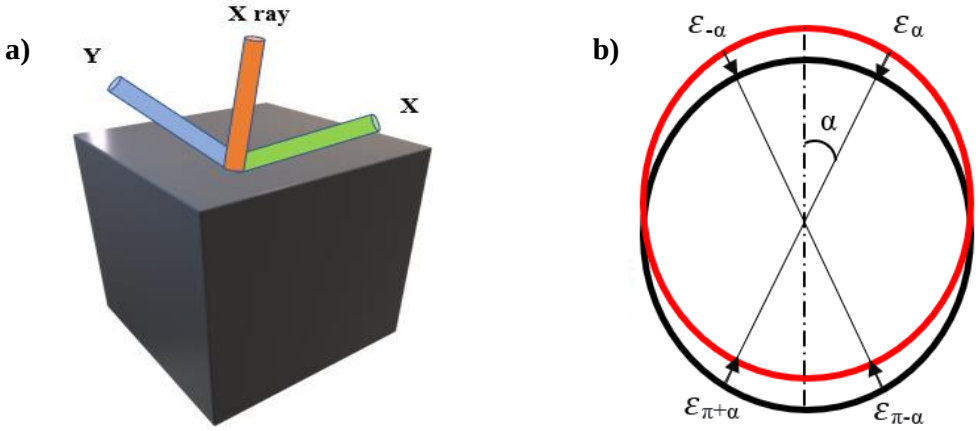

Figure 1: (a) Demonstration of in-plane residual stress(σ_x)and shear residual stress (τ_{xy}) direction on a sample surface and (b) schematic of Debye-Scherrer ring position of L-PBF samples (red ring) and wrought (black ring) Inconel 625 samples with four strains (ε) shown.

$$\varepsilon_{\alpha 1} = \frac{1}{2}\{(\varepsilon_{\alpha} - \varepsilon_{\pi+\alpha}) + (\varepsilon_{-\alpha} - \varepsilon_{\pi-\alpha})\} \quad (2)$$

$$\varepsilon_{\alpha 2} = \frac{1}{2}\{(\varepsilon_{\alpha} - \varepsilon_{\pi+\alpha}) - (\varepsilon_{-\alpha} - \varepsilon_{\pi-\alpha})\} \quad (3)$$

$$\sigma_x = -\frac{E}{1+\nu} \cdot \frac{1}{sin2\eta} \cdot \frac{1}{sin2\varphi_o} \cdot \left(\frac{\partial \varepsilon_{\alpha 1}}{\partial cos\alpha}\right) \quad (4)$$

$$\tau_{xy} = \frac{E}{2(1+\nu)} \cdot \frac{1}{sin2\eta} \cdot \frac{1}{sin\varphi_o} \cdot \left(\frac{\partial \varepsilon_{\alpha 2}}{\partial sin\alpha}\right) \quad (5)$$

where $\varepsilon_{\alpha 1}$ is the mean of the four principal strains, $\varepsilon_{\alpha 2}$ is the mean difference of the four principal strains as shown in Fig 1 (b), while *E* and ν are the Young's modulus and Poisson's ratio of Inconel 625, respectively. Vickers micro-indentations were made along the top surface of the as-built and heat-treated samples using a Phase II 900-391D hardness tester. A total of 5 indentations were performed along each sample's face and an average was calculated along with standard deviation. Indentations were made using a load of 1 kgf with a dwell time of 15 secs.

Results and Discussion

The Vickers microhardness values of the as-built and three heat-treated L-PBF Inconel 625 samples are presented in Fig. 2. It was found that the as-built sample had the highest hardness value of 364 ± 1.17 HV. The presence of tensile residual stress, fine dendritic microstructure, high dislocation density arising from complex thermal gradients during the printing process, and entrapment of heavy atoms like Molybdenum (Mo) and Niobium (Nb) along sub-grain domain boundaries, are possible reasons for it being higher than the as-received (AR) wrought material hardness which was 243.85 ± 1.15 HV. Higher heat-treatment temperatures led to lower microhardness values due to softening. The microhardness values of the 700 ^{o}C, 900 ^{o}C, 1050 ^{o}C heat-treated samples were 361 ± 3.21 HV, 314 ± 0.66 HV, 255 ± 1.88 HV, respectively. Similar results have been observed in the literature [18]. Possible reasons behind this decreasing trend in microhardness could be the reduction in dislocation density, dissolution of heavy atoms like Mo and Nb trapped along the grain boundaries, etc. At

1050 °C, the sample is considered to attain complete recrystallization of grains with no heavy atoms or secondary phases present in the microstructure.

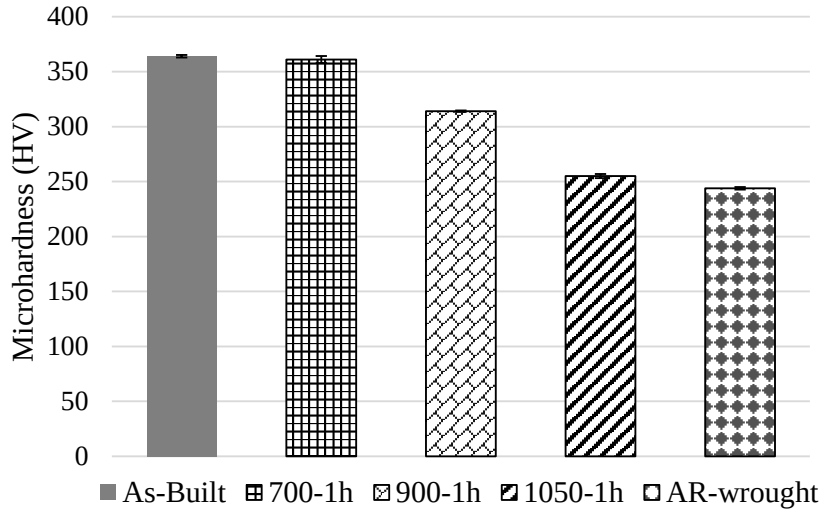

Figure 2: Microhardness of as-built and heat-treated L-PBF Inconel 625 samples. Error bars denote standard deviation.

Residual stress values and nature (tensile or compressive) determined using the cos α method along the top surface of the as-built and heat-treated L-PBF Inconel 625 samples are shown in Fig. 3. As seen from Fig. 3, the top surface of the as-built sample is dominated by tensile residual stress with a value of 77 ± 15 MPa. This tensile residual stress is generated from the complex thermal gradients and rapid cooling rates (in range of 10^3 K/s to 10^6 K/s) occurring during the L-PBF process. The intense cooling related to the laser leaving the melt pool and freshly coated powder layers causes built layers under the exposed surface to shrink. Shrinkage of newly added layers is accompanied by an additional rise in tensile residual stress. Similar results were reported by Shuai et al. where they observed formation of intense tensile residual stress in as-built SLM Inconel 625_samples[19]. Heat treatments performed herein reduced as-built tensile residual stress. Increasing the heat-treatment temperature reduced the tensile residual stress and increased the formation of compressive residual stress on the surface. For 700 °C, 900 °C, and 1050 °C samples, the residual stresses were measured as -64 ± 13 MPa, -96 ± 17 MPa, and -394 ± 50 MPa, respectively. Similar effects of stress relieved heat treatment on residual stress were observed in L-PBF Inconel 718 where tensile residual stress was removed and compressive residual stress was formed on the surface [5]. Formation of high compressive stress on a surface has proven to improve the fatigue life, fatigue strength, slow crack propagation, and increase resistance to environmentally assisted cracking, such as stress corrosion cracking of the material in past studies [20]. The high standard deviation in the 1050 °C heat-treated sample is an indication of an increase in grain size. Since the grain size is large, the number of grains taken into consideration under one incident angle X-ray exposure is less and this led to large uncertainty.

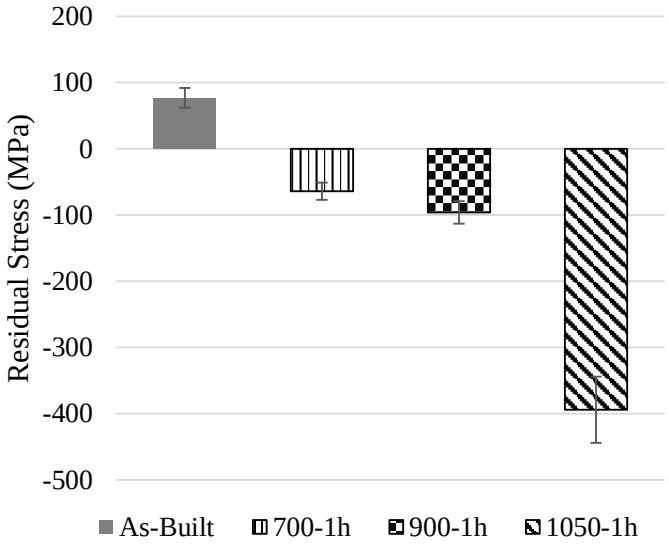

Figure 3: Residual stress of as-built and heat-treated L-PBF Inconel 625 samples. Positive values represent tensile and negative values represent compressive residual stress. Error bars provide the standard deviation.

The D-S ring distortion and (311) peak of the as-built, 700 ºC, 900 ºC, and 1050 ºC heat-treated samples are shown in Fig. 4. The D-S ring, which is recorded on a two-dimensional detector, is taken by the single exposure of X-rays, and this is an important working principle of the cos α method. As seen in Fig. 4, the ring distortion from the standard D-S ring position can be used to understand the nature and value of residual stress. The white lines in Fig 4 (lines appear as 'cross-hairs') indicate the position of a wrought Inconel 625 D-S ring position. Tensile residual stress within a sample shifts the D-S ring position below the white lines. The presence of compressive residual stress moves the D-S ring position above the white lines. The intensity uncertainty of the (311) diffraction peak is maximum for the 1050 ºC heat-treated sample which may be due to larger grain size. The intensity uncertainty is less for fine grains observed in the as-built L-PBF samples. A similar level of uncertainty is observed in the residual stress results in Figure 3. The FWHM of the (311) diffraction peak for as-built, 700 ºC, 900 ºC, and 1050 ºC samples were quantified as 2.98 ± 0.11, 2.78 (+0.09/-0.14), 2.84 ± 0.09, 3.99 (+0.56/-0.42) degrees, respectively. The reduction of the FWHM of the diffraction peak from the as-built condition to 700 ºC provides an indication of micro strain relaxation in grains. In 900 ºC heat-treated sample, the FWHM increases slightly implying the possible formation of metastable δ precipitate in finer quantity. Precipitates are one source for forming strains [21].

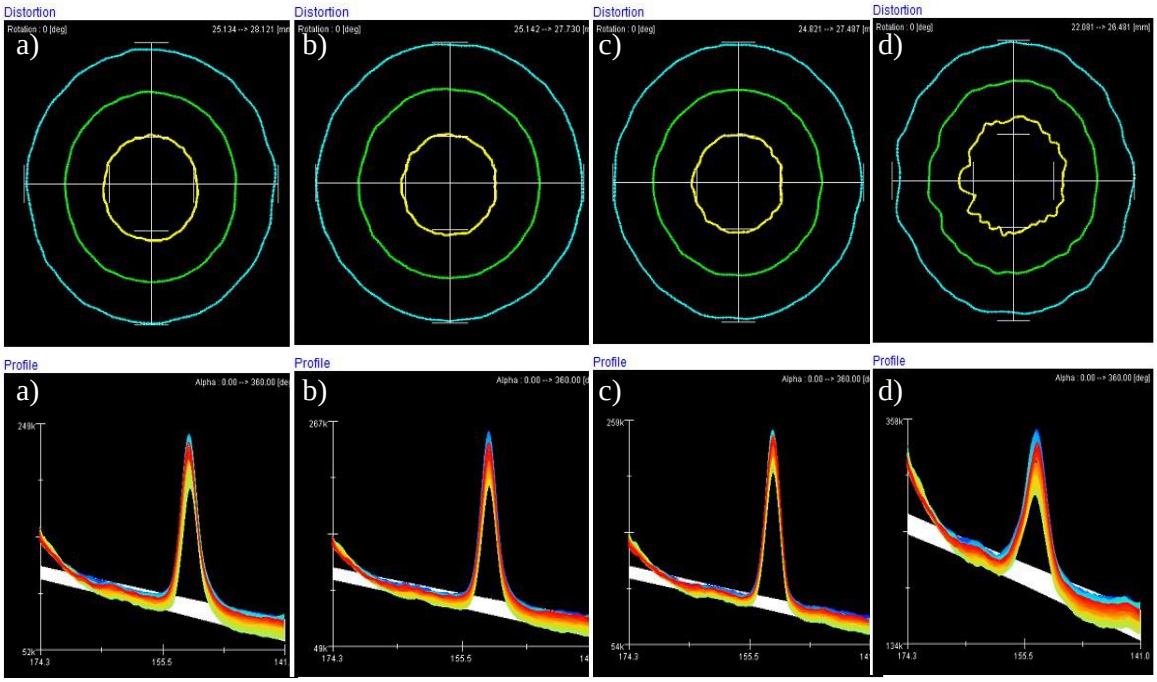

Figure 4: (top row) Debye-Scherrer ring distortion and (bottom row) (311) diffraction peak profiles of (a) as-built, (b) 700 ºC (c) 900 ºC, and (d) 1050 ºC L-PBF Inconel 625 samples.

Figure 5 shows the cos α and sin α diagrams of the as-built, 700 ºC, 900 ºC, and 1050 ºC L-PBF Inconel 625 samples. Note that the slope of the fitting red line and elastic constant indicates residual stress (σ_x) in the cos α plots and the slope of the fitting red line and elastic constant indicates shear stress (τ_{xy}) in the sin α plots. In the as-built Inconel 625 sample, the presence of tensile residual stress provides for a negative slope, i.e., -0.000166, in the cos α diagram. In all heat-treated samples, the presence of compressive residual stress provides for positive slopes in the cos α diagrams. For the 700 ºC, 900 ºC, and 1050 ºC heat-treated samples, the cos α diagram slope was 0.000138, 0.000208, and 0.000853, respectively. In addition, the presence of positive shear stress in all samples provides for a positive slope in the sin α diagrams. For the as-built, 700 ºC, 900 ºC, and 1050 ºC samples, the sin α diagram slopes were 0.000037, 0.000048, 0.000029, and 0.000176, respectively. The shear stress values measured in the as-built, 700 ºC, 900 ºC, and 1050 ºC are 15$\pm$10, 19$\pm$13, 12$\pm$19, and 70$\pm$74 MPa, respectively. These results are consistent with the study conducted by Tanaka which mentions negative slopes in the cos α diagram indicate the presence of tensile residual stress and positive slopes in the sin α diagram indicate the presence of positive shear stress [12].

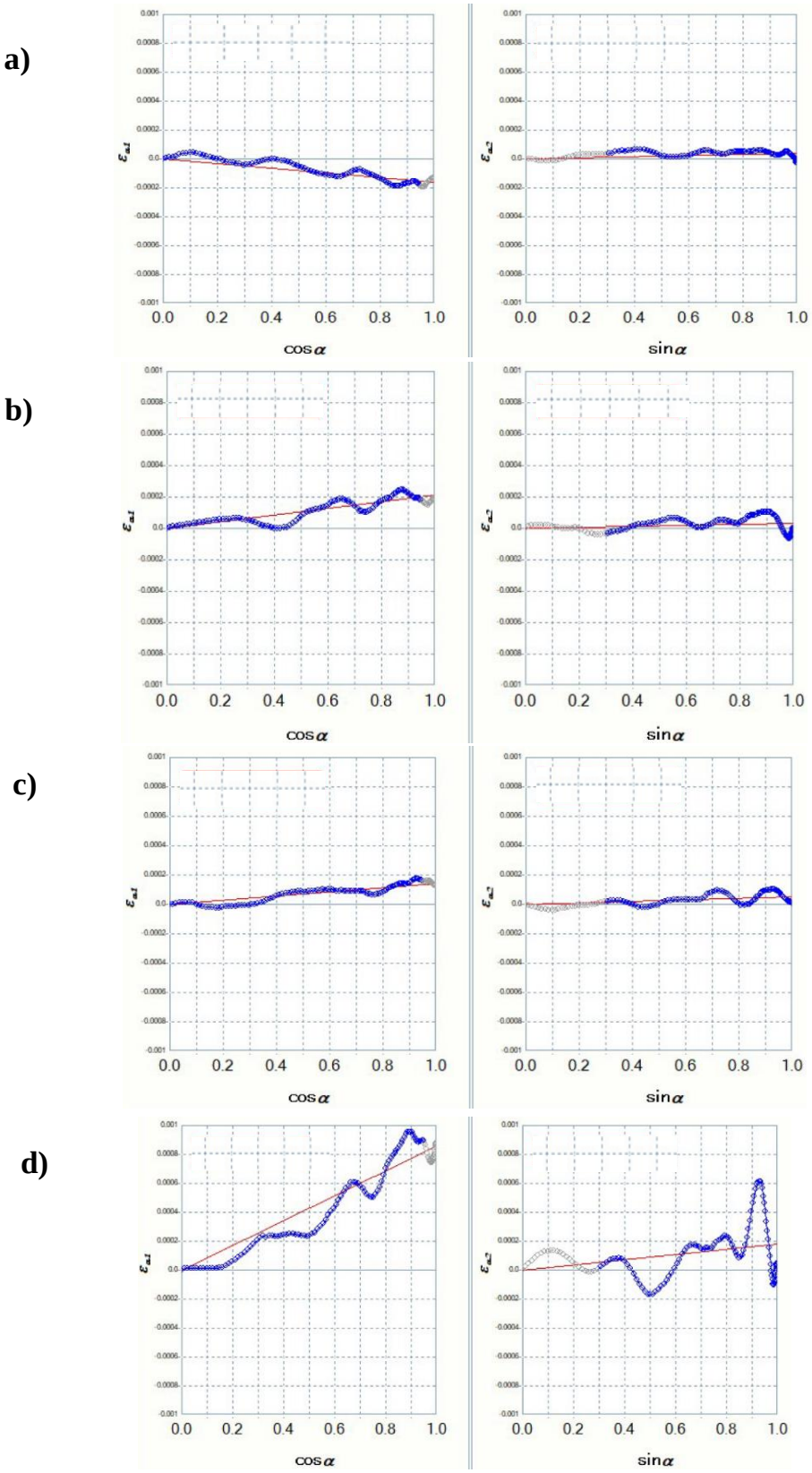

Figure 5: Cos α and sin α diagrams of (a) as-built, (b) 700 ºC, (c) 900 ºC, and (d) 1050 ºC L-PBF Inconel 625 samples.

The interrelationship between the residual stress and microhardness of the as-built, 700 ºC, 900 ºC, and 1050 ºC L-PBF Inconel 625 samples are shown in Fig. 6. It may be seen that both residual stress and microhardness trends are positively correlated. The decrease in microhardness indicates a decrease in strength. The decrease in microhardness with increasing heat-treatment temperature is an indication of tensile residual stress relaxation. At 700 ºC, the sample goes through a stress relief heat treatment. Relaxation of tensile residual stress reduces the microhardness. On the surface where compressive residual stress is dominating, the microhardness is expected to be maximum because of compressed grains making it difficult to deform under external force. However, the microhardness observed in this case is minimum for the sample heat treated at 1050 ºC, as microhardness indentation strains goes deeper than the surface or near surface area. Possible reasons for this observation could be reduction of dislocation density, dissolution of intermetallic phases like γ" and δ, recrystallization of grains, and reduction in anisotropy. Intermetallic phases γ" and δ are generally made of Nb and Mo heavy atoms. Dissolution of these heavy atoms back in the γ-matrix decreases the microhardness of a sample. The decreasing trend of microhardness with respect to increase in heat-treatment temperature was also seen in a study conducted by C. Li et al [18].

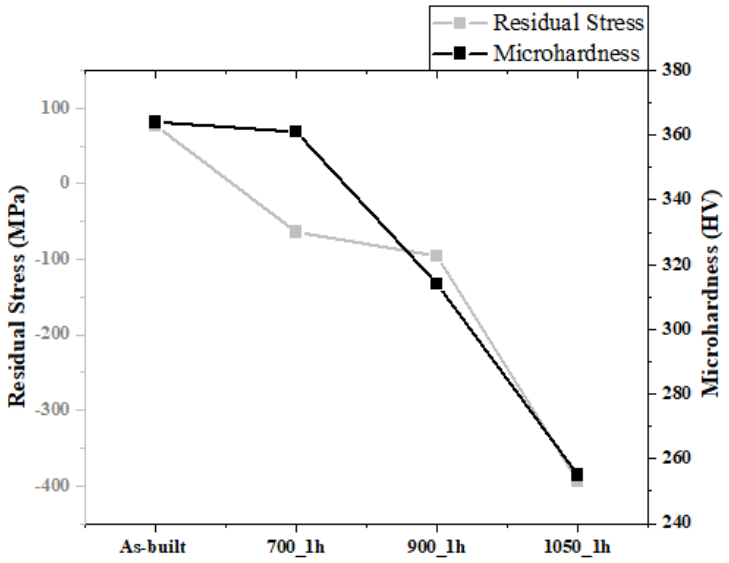

Figure 6: Residual stress and microhardness of as-built and heat-treated L-PBF Inconel 625 samples.

Conclusions

In this study, the measurement of surface residual stress and microhardness of as-built and heat-treated Inconel 625 specimens fabricated via L-PBF was conducted. An XRD system that integrates the cos α method was used to determine residual stress values in the specimens. The primary findings from this study are summarized below:

- The as-built L-PBF Inconel 625 exhibited high tensile residual stress (77± 15 MPa) and the highest microhardness (364 ± 1.17 HV). The tensile residual stress is a direct result of the L-PBF layer-by-layer manufacturing process in which thermal gradients in the build-wise direction are high. The high microhardness is attributed to the very fast cooling rates experienced during L-PBF – resulting in fine, hard microstructures.

- Heat treating the as-built samples at 700 ^{o}C for 1 hour resulted in transformation of detrimental tensile residual stress (77 ± 15 MPa) to beneficial compressive residual stress (-64 ± 13 MPa).
- Microhardness and tensile residual stress both decrease with increasing heat-treatment temperature.
- Increasing the heat-treatment temperature from 700 ^{o}C to 900 ^{o}C resulted in the compressive residual stress increasing by 50%, i.e., from -64 ± 13 MPa to -96 ± 17 MPa. This could be an indicator of precipitates ($\gamma''$and δ) beginning their dissolution back in Ni-Cr matrix.
- For the 1050 ^{o}C L-PBF Inconel 625 sample, the top surface demonstrated extensive compressive residual stress which subsequently enhances the fatigue life, fatigue strength, and slows the crack propagation. At this temperature, complete dissolution of all precipitates occurs which may be a major contributor to compressive residual stress along the surface.
- Debye-Scherrer ring distortion from standard wrought white lines was used to determine strain and ultimately residual stress. Tensile residual stress in a sample moved the D-S ring below the white lines. On the other hand, compressive residual stress moved the D-S ring above the white line.

The cos α method provides a unique means for measuring residual stress in different materials built using different AM or conventional machining processes. The results presented in this study provide insight into how heat treatment affects surface residual stress and microhardness simultaneously in L-PBF Inconel 625.

Acknowledgement

This material is based upon work supported by the U.S. Department of Energy's Office of Nuclear Energy under Award Number DE-NE0008865.

Disclaimer

References

[1] D. M. D'Addona, S. J. Raykar, and M. M. Narke, "High Speed Machining of Inconel 718: Tool Wear and Surface Roughness Analysis," *Procedia CIRP*, vol. 62, pp. 269–274, 2017, doi: 10.1016/j.procir.2017.03.004.

[2] K. Mahesh, J. T. Philip, S. N. Joshi, and B. Kuriachen, "Machinability of Inconel 718: A critical review on the impact of cutting temperatures," *Materials and Manufacturing*

Processes, vol. 36, no. 7, pp. 753–791, 2021, doi: 10.1080/10426914.2020.1843671.

[3] X. Wang and K. Chou, "Residual stress in metal parts produced by powder-bed additive manufacturing processes," *Proceedings - 26th Annual International Solid Freeform Fabrication Symposium - An Additive Manufacturing Conference, SFF 2015*, pp. 1463–1474, 2020.

[4] F. Liu, X. Lin, G. Yang, M. Song, J. Chen, and W. Huang, "Microstructure and residual stress of laser rapid formed Inconel 718 nickel-base superalloy," *Optics & Laser Technology*, vol. 43, no. 1, pp. 208–213, 2011, doi: https://doi.org/10.1016/j.optlastec.2010.06.015.

[5] R. Barros *et al.*, "Stress Analysis Before and After Heat Treatment," *Metals*, vol. 9, no. 12, p. 1290, 2019, [Online]. Available: https://www.mdpi.com/2075-4701/9/12/1290.

[6] Y. Liu, Y. Yang, and D. Wang, "A study on the residual stress during selective laser melting (SLM) of metallic powder," *International Journal of Advanced Manufacturing Technology*, vol. 87, no. 1–4, pp. 647–656, 2016, doi: 10.1007/s00170-016-8466-y.

[7] L. Parry, I. A. Ashcroft, and R. D. Wildman, "Understanding the effect of laser scan strategy on residual stress in selective laser melting through thermo-mechanical simulation," *Additive Manufacturing*, vol. 12, pp. 1–15, 2016, doi: 10.1016/j.addma.2016.05.014.

[8] J. Zhang, S. Li, Q. Wei, Y. Shi, L. Wang, and L. Guo, "Cracking behavior and inhibiting process of inconel 625 alloy formed by selective laser melting," vol. 39, pp. 961–966, 2015, doi: 10.13373/j.cnki.cjrm.2015.11.001.

[9] D. Deng, R. L. Peng, H. Brodin, and J. Moverare, "Microstructure and mechanical properties of Inconel 718 produced by selective laser melting: Sample orientation dependence and effects of post heat treatments," *Materials Science and Engineering A*, vol. 713, no. July 2017, pp. 294–306, 2018, doi: 10.1016/j.msea.2017.12.043.

[10] J. Guo, H. Fu, B. Pan, and R. Kang, "Recent progress of residual stress measurement methods: A review," *Chinese Journal of Aeronautics*, vol. 34, no. 2, pp. 54–78, 2020, doi: 10.1016/j.cja.2019.10.010.

[11] M. Masoomi *et al.*, "Residual stress measurements via neutron diffraction of additive manufactured stainless steel 17-4 PH," *Data in Brief*, vol. 13, 2017, doi: 10.1016/j.dib.2017.06.027.

[12] K. Tanaka, "The cosα method for X-ray residual stress measurement using two-dimensional detector," *Mechanical Engineering Reviews*, vol. 6, no. 1, pp. 18-00378-18–00378, 2019, doi: 10.1299/mer.18-00378.

[13] S. X. Elastic, "Comparison of Two X-Ray Residual Stress Measurement Methods: Sin2 ψ and Cos α, Through the Determination of a Martensitic Steel X-Ray Elastic Constant," *Residual Stresses 2016*, vol. 2, no. January 2017, pp. 55–60, 2017, doi: 10.21741/9781945291173-10.

[14] T. Oguri, T. Tanaka, T. Okano, K. Murata, H. Kawakami, and Y. Sato, "X-ray Stress Measurement of the Cylindrical Surface by the cos α Method," *Journal of the Society of Materials Science, Japan*, vol. 66, pp. 488–494, 2017, doi: 10.2472/jsms.66.488.

[15] M. R. Stoudt *et al.*, "The Influence of Annealing Temperature and Time on the Formation of δ-Phase in Additively-Manufactured Inconel 625," *Metallurgical and*

Materials Transactions A: Physical Metallurgy and Materials Science, vol. 49, no. 7, pp. 3028–3037, 2018, doi: 10.1007/s11661-018-4643-y.

[16] T. Sasaki, Y. Hirose, K. Sasaki, and S. Yasukawa, "Influence of image processing conditions of Debye Scherrer ring images in X-ray stress measurement using an imaging plate ," *JCPDS-International Centre for Diffraction Data*, no. C, 1997.

[17] K. Siang, "Effect of Residual Stress and Cold Work on Fatigue of Inconel 718 - Final.pdf," 2019.

[18] C. Li, R. White, X. Y. Fang, M. Weaver, and Y. B. Guo, "Microstructure evolution characteristics of Inconel 625 alloy from selective laser melting to heat treatment," *Materials Science and Engineering A*, vol. 705, no. August, pp. 20–31, 2017, doi: 10.1016/j.msea.2017.08.058.

[19] L. Shuai, Q. Wei, Y. Shi, J. Zhang, and L. Wei, "Micro-crack formation and controlling of Inconel625 parts fabricated by selective laser melting," *Solid Freeform Fabrication 2016: Proceedings of the 27th Annual International Solid Freeform Fabrication Symposium - An Additive Manufacturing Conference, SFF 2016*, pp. 520–529, 2016.

[20] L. H. Wu and C. H. Jiang, "Effect of shot peening on residual stress and microstructure in the deformed layer of Inconel 625," *Materials Transactions*, vol. 58, no. 2, pp. 164–166, 2017, doi: 10.2320/matertrans.M2016298.

[21] T. Ungár, "Microstructural parameters from X-ray diffraction peak broadening," *Scripta Materialia*, vol. 51, no. 8 SPEC. ISS., pp. 777–781, 2004, doi: 10.1016/j.scriptamat.2004.05.007.